Optimizing 4D Cone Beam Computed Tomography Acquisition by Varying the Gantry Velocity and Projection Time Interval

Ricky T O'Brien[1], Benjamin J Cooper[1,2] and Paul J Keall[1]

[1] Radiation Physics Laboratory, Sydney Medical School, The University of Sydney, NSW 2006, Australia.

[2] Department of Medical Physics, The Canberra Hospital, ACT 2605, Australia.

E-mail: ricky.obrien@sydney.edu.au

Abstract. Four Dimensional Cone Beam Computed Tomography (4DCBCT) is an emerging clinical image guidance strategy for tumour sites affected by respiratory motion. In current generation 4DCBCT techniques, both the gantry rotation speed and imaging frequency are constant and independent of the patient's breathing which can lead to projection clustering. We present a Mixed Integer Quadratic Programming (MIQP) model for Respiratory Motion Guided-4DCBCT (RMG-4DCBCT) which regulates the gantry velocity and projection time interval, in response to the patient's respiratory signal, so that a full set of evenly spaced projections can be taken in a number of phase, or displacement, bins during the respiratory cycle. In each respiratory bin, an image can be reconstructed from the projections to give a 4D view of the patient's anatomy so that the motion of the lungs, and tumour, can be observed during the breathing cycle. A solution to the full MIQP model in a practical amount of time, 10 seconds, is not possible with the leading commercial MIQP solvers, so a heuristic method is presented. Using parameter settings typically used on current generation 4DCBCT systems (4 minute image acquisition, 1200 projections, 10 respiratory bins) and a patient with a four second breathing period, we show that the root mean square (RMS) of the angular separation between projections with displacement binning is 2.7° using existing constant gantry speed systems and 0.6° using RMG-4DCBCT. For phase based binning the RMS is 2.7° using constant gantry speed systems and 2.5° using RMG-4DCBCT. The optimization algorithm presented is a critical step on the path to developing a system for RMG-4DCBCT.

1. Introduction

Lung cancer is the leading cause of cancer related death worldwide (18%) with 1.2 million new cases reported annually (Boyle & Levin 2008). Despite 36% to 71% of lung cancer patients receiving radiotherapy (Delaney et al. 2005), and continous efforts to improve treatment outcomes, the 5 year survival rate is only 16% (American Cancer Society 2008, Cancer Facts and Figures). These patients urgently need better treatment techniques and tools to improve survival rates.

An increase in the biologically effective tumour dose of 1-Gy results in a 4% improvement in survival (Machtay et al. 2012). On the other hand, a 1-Gy decrease in overall mean lung dose results in a 2% reduction in pneumonitis (Marks et al. 2010). It is clear from these statistics that better targeted radiotherapy has the potential to improve treatment outcomes. Image-guided radiotherapy (IGRT) has been used to simultaneously increase tumour dose while minimising the dose to the surrounding healthy tissue. IGRT is used by more than 93% of radiation oncologists in the United States (Simpson et al. 2010). However, imaging techniques such as MRI, PET, CT and CBCT are blurry or contain artifacts when there is significant respiratory motion. As a consequence, it is difficult for a radiotherapist to accurately position their patient's for treatment which increases the likelihood that some of the radiation that is targeted at the tumour will irradiate healthy lung tissue. An additional complication, is that although the tumour is being treated with radiation, imaging techniques deliver radiation to the parts of the patients anatomy that are being imaged. Radiotherapists must balance the increased radiation delivered to the patient from imaging with the reduction in treatment margins expected from the use of the imaging technique.

CBCT images can be obtained using the kilovoltage imagers attached to linear accelerators and are used in the treatment room by radiotherapists to position their patients for treatment. The gantry, containing the X-ray source and detector, is rotated around the anatomy during which a series of approximately 1200 cone shaped projections are taken, see figure 1. The projections are then reconstructed using the Feldkamp-Davis-Kress (FDK) algorithm to give a 3D view of the patient's anatomy (Feldkamp et al. 1984).

4DCBCT provides a video, or movie, of the patient's anatomy. The motion of the abdomen, lungs and tumour can be observed during the breathing cycle. To acquire 4D images, the respiratory cycle is separated into respiratory bins such as inhale limit, exhale limit and at different stages between the two limits. For 4DCBCT imaging a full set of projections are collected in each respiratory bin so that a four dimensional view of the changing anatomy can be obtained. First generation 4DCBCT was published between 2003 and 2005 (Taguchi 2003, Sonke et al. 2005), with the first clinical release in 2010 by Elekta (Stockholm Sweden).

In this paper we describe why projections are clustered during 4DCBCT image acquisition. We introduce a novel Mixed Integer Quadratic Programming (MIQP) optimization model for Respiratory Motion Guided 4DCBCT (RMG-4DCBCT) that

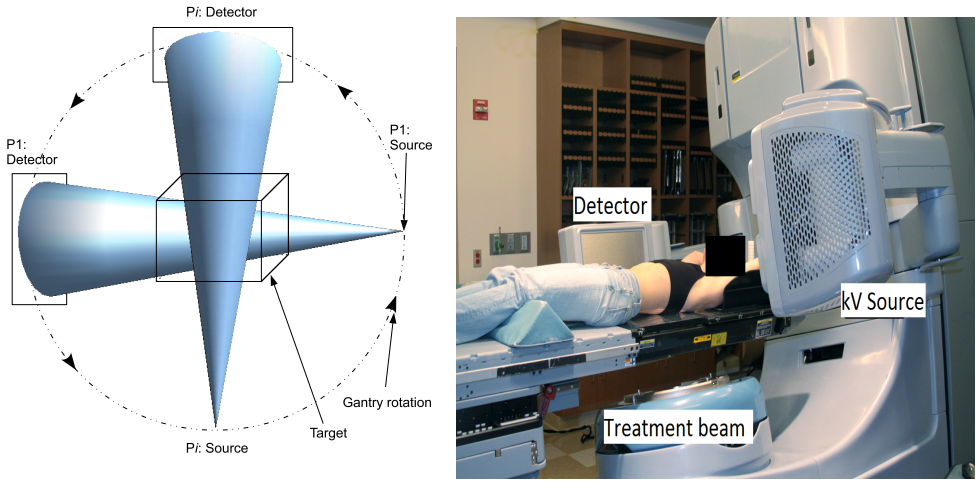

Figure 1. Left (A): Diagram of the projection geometry for CBCT imaging showing the first (P1) projection and $i^{\text{th}}(\text{P}_i)$ projection. The gantry rotates around the target at a constant velocity with a constant pulse rate between projections. Right (B): A photograph of a linear accelerator used in radiotherapy with the kilovoltage imager.

regulates the gantry velocity and projection time interval with the aim of reducing the variability of the angular separation between projections compared to conventional 4DCBCT techniques.

2. 4DCBCT Projection Clustering

4DCBCT imaging attempts to produce images showing the motion of the lungs, and tumour, during the breathing cycle. The aim is to collect enough projections in each respiratory bin, with relatively even angular separation, to reconstruct an image. Within each respiratory bin, there is limited anatomical motion, so blurring and artefacts in the resulting image are reduced. Three dimensional images are reconstructed in each respiratory bin and a video is created showing a 4D view of the anatomy.

Common to all current 4DCBCT systems is the use of a constant angular velocity of the gantry with a constant projection pulse rate. The gantry is rotated around the patient at a much slower rate than for 3DCBCT imaging. After the projections have been collected, they are compared with the recorded breathing trace, which is either derived from the images themselves or a respiratory sensor (e.g the Real-Time Position Management (RPM) system from Varian Medical Systems), and then post-processed into respiratory bins.

The use of a constant angular velocity results in clustering of projections. Figure 2 is an example of projection clustering using parameter settings typically used with the current generation of 4DCBCT systems from Elekta. In this example a sinusoidal breathing wave is used for a patient with a four second breathing period. The x-axis tick marks correspond to the time at which a projection is taken if a pulse rate of 0.2s is used. The projections corresponding to displacement bins 1, 5 and 8 are marked in

cyan, green and magenta respectively. If the gantry is rotated with an angular velocity of 1.5°/s and a projection is taken every 0.2 seconds there will be 1200 projections in total taken over 4 minutes. If we analyse the displacement bin at exhale limit (cyan), then either 4 or 5 projections, with an angular separation of 0.9° to 1.2°, will be taken in the 0.82 seconds at exhale limit. The patient's breathing will not enter the exhale limit respiratory bin for a further 3.18 seconds in which time the gantry moves 4.77°. This process will be repeated with a cluster of 4 or 5 projections followed by a gap of at least 4.77° before the next cluster of projections. A polar plot showing the gantry angle for each projection in displacement bin 1 is the cyan polar plot in figure 2. In total there will be 240 projections in 60 clusters if 4 projections are taken per respiratory bin. In the worst case scenario there will be 5 projections per respiratory bin resulting in 300 projections in displacement bin 1.

Clustering of projections results in a higher radiation dose to the patient for a small improvement in image quality as the clustered projections provide similar information on the patients anatomy. In addition, it has been reported that streak artefacts occur due to the clustering of projections using the FDK algorithm (Leng et al. 2008).

The green polar plot in figure 2 shows an example of missed projections. Even though the polar plot has a consistent angular separation between projections, only one projection exists per respiratory cycle. The patient has received a radiation dose from 60 projections but there may not be enough projections to reconstruct an image of suitable quality. This problem occurs because only 0.13 seconds is spent in displacement bin 5 during inhale and a further 0.13 seconds during exhale. A 0.2 second projection pulse rate can miss the displacement bin altogether. In our example a projection is taken during exhale but not during inhale. In an extreme case, the displacement bin can be missed during both inhale and exhale in consecutive cycles leading to large gaps between projections. In the worst case, the respiratory bin could be missed during both inhale and exhale resulting in no projections allocated to respiratory bin 5. Although the missed projections could be sourced from a neighbouring respiratory bin, for optimal image quality it is desirable to have all projections corresponding to the same respiratory bin.

The magenta polar plot in figure 2 has a projection taken during both inhale and exhale, resulting in 120 projections in total, but the projections are unevenly spaced. For displacement bin 8 there may be enough projections to reconstruct an image, but if the projections were more evenly spaced fewer projections would be required to obtain an image with comparable quality.

3. Respiratory Motion Guided-4DCBCT (RMG-4DCBCT)

The aim of RMG-4DCBCT is to improve the angular separation between projections. To do this, we use two additional degrees of freedom over current generation 4DCBCT methods. The first degree of freedom is that rather than moving the gantry with a constant angular velocity, we allow the motion of the gantry to be regulated within

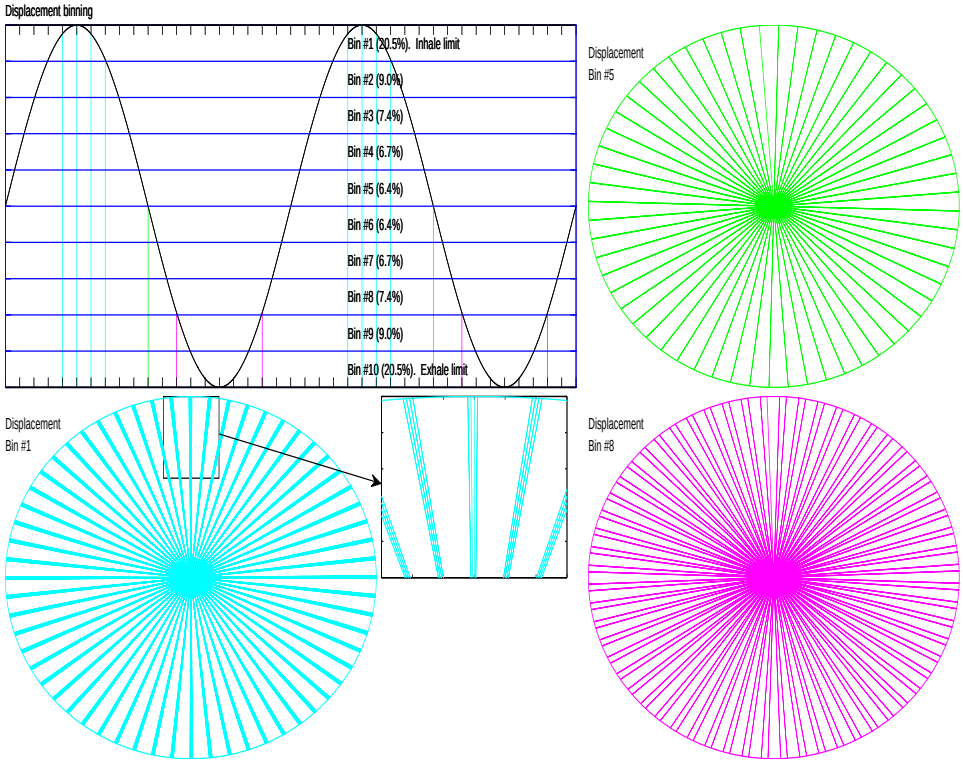

Figure 2. Example of clustered and missing projections with a sinusoidal breathing wave and a four second breathing period. Top left: The patient's breathing wave with displacement on the vertical axis and time on the horizontal axis where the breathing cycle is separated into 10 displacement bins. The percentages listed are the approximate percentages of time spent in each displacement bin. The cyan, green and magenta vertical lines correspond to projections that are allocated to respiratory bins 1, 5 and 8 respectively. The polar plots show the gantry angles at the projections taken in respiratory bins 1 (cyan), 5 (green) and 8 (magenta) with a constant gantry velocity of 1.5°/s.

specified limits on maximum velocity and acceleration. The second degree of freedom is that rather than using a constant projection pulse rate we allow the time interval between projections to be varied.

The optimization model presented in this paper is just one aspect of a larger project with the aim of developing a system that implements RMG-4DCBCT. A flowchart of the process is given in figure 3. The patient's breathing pattern is analysed and a representative breathing trajectory is determined. We use the representative breathing trajectory to compute the gantry velocity and projection time interval schedule using (MIQP) techniques. We then monitor the patient's breathing, moving the gantry according to the real time breathing signal, to acquire the projections.

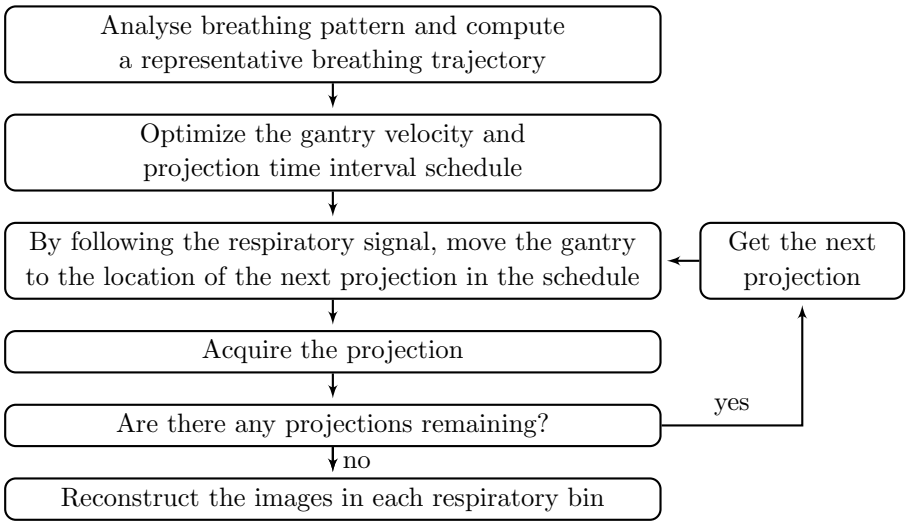

Figure 3. A flowchart showing the main algorithm controlling RMG-4DCBCT.

4. Optimizing the Gantry Velocity and Projection Time Interval Schedule

Our initial focus is on the problem formulation without consideration of computational efficiency. After formulating the problem, we will present a heuristic solution method that produces a near optimal solution in under one second. As this is the first article describing RMG-4DCBCT optimization, we will give a full detailed description of the constraints rather than just listing them. To make the discussion easier to follow, we will break the model into smaller components and discuss each in detail in the remainder of this section.

4.1. Pre-processing to determine the time windows

We use respiratory bins within which there is negligible anatomic motion. The bins can be based either on displacement or phase of the lungs or abdomen as measured by a respiratory sensor. Once we obtain the patient's breathing signal, we use it to compute a set of time windows, $R_{b,j}$, which define the estimated entry and exit times for each respiratory bin:

$$R_{b,j} = \{ts_{b,j}, te_{b,j}\} \text{ for } b = 1, 2, \ldots, N \text{ and } j = 1, \ldots, N_b, \tag{1}$$

where b is the b^{th} respiratory bin, j is the j^{th} time that the patient's breathing has entered respiratory bin b, $ts_{b,j}$ is the start or entry time for the time window, $te_{b,j}$ is the exit time for the time window, N_b is the number of time windows for bin b and N is the number of respiratory bins. The time windows are computed numerically in a pre-processing stage before image acquisition starts. Projections taken between $ts_{b,j}$ and $te_{b,j}$ must be allocated to respiratory bin b and used to reconstruct the image for respiratory bin b.

4.2. Constraints on the minimum time between projections

If we assume that the time interval between projections, Δt_k, is to be determined as part of the optimization and a projection is taken at time t_k, then we have the following equations and constraints governing time:

$$t_{k+1} = t_k + \Delta t_k \text{ for } k = 1, 2, \ldots, M-1,$$
$$\Delta t_k \geq \Delta t_{min} \text{ for } k = 1, 2, \ldots, M,$$

where $M = \sum_{b=1}^{N} M_b$ is the total number of projections taken, M_b is the number of projections taken in respiratory bin b and $t_M = t_{max}$ is the total image acquisition time. The minimum time, Δt_{min}, is the minimum time required for the detector to be ready to record a second projection after taking a projection. This is an input into the optimization and needs to be measured for each CBCT device. Current generation scanners are capable of a projection frequency of greater than 10hz, so a value of $\Delta t_{min} = 0.1$ will be used.

4.3. Constraints to sort projections into respiratory bins

If the time span between projections is constant, then we can assign the projections to respiratory bins in a pre-processing phase. Unfortunately, assigning projections to respiratory bins is much more difficult when the time span between projections is a decision variable. To determine the respiratory bin that the projection taken at time t_k belongs, we introduce binary variables $\delta_{b,j,k}$ which take the value 1 if t_k is in time window $R_{b,j}$ and zero otherwise:

$$ts_{b,j}\delta_{b,j,k} \leq t_k \leq te_{b,j} + (1 - \delta_{b,j,k})\, t_{max} \text{ for all } b, j \text{ and } k,$$
$$\sum_{b=1}^{N}\sum_{j=1}^{N_b} \delta_{b,j,k} = 1 \text{ for all } k,$$
$$\sum_{j=1}^{N_b} \delta_{b,j,k} = \delta_{b,k} \text{ for all } b \text{ and } k,$$
$$\sum_{k=1}^{M}\sum_{j=1}^{N_b} \delta_{b,j,k} = M_b \text{ for all } b, \tag{2}$$

where $\delta_{b,k}$ is 1 if the projection taken at time t_k is in respiratory bin b and zero otherwise. Constraint 2 guarantees that projections are not missed and that exactly M_b projections are taken in respiratory bin b.

4.4. Constraints on the motion of the gantry

For half fan acquisition the gantry rotates between 0° and 360°. When the gantry hits either 0° or 360° it must stop or change direction. Let θ_k be the position of the gantry for the projection taken at time t_k, then the limits on the gantry angle can be modelled with:

$$0 \leq \theta_k \leq 2\pi \text{ for all } k.$$

For full fan acquisition the gantry can rotate from 0° to 180°, plus the fan angle, ω, so we apply

$$0 \leq \theta_k \leq \pi + \omega \text{ for all } k.$$

The gantry has mechanical constraints on maximum velocity and maximum acceleration. The maximum velocity, $\dot{\theta}_{max}$, in the clockwise direction can be different to the maximum velocity in the anticlockwise direction. However, for safety reasons, the International Electrotechnical Commission (I.E.C) specifies a limited of $6^\circ/s$ on the velocity of the gantry. We model the maximum velocity constraint with

$$|\theta_{k+1} - \theta_k| \leq \dot{\theta}_{max}\Delta t_k \text{ for all } k. \tag{3}$$

Maximum acceleration, $\ddot{\theta}_{max}$, is influenced by gravity and other mechanical constraints with the values varying with gantry angle. Values for acceleration have been measured at between $1.8^\circ/s^2$ and $3.2^\circ/s^2$, with deceleration measured at between $3.4^\circ/s^2$ and $4.3^\circ/s^2$ for the Elekta Synergy linear accelerator (Boylan et al. 2011). Values for acceleration and deceleration for non emergency stops on Varian Medical Systems TrueBeam are around $12^\circ/s^2$ ‡. In this study, to simplify the model, we will assume that the maximum acceleration is a constant for all gantry angles. Modelling the acceleration is achieved by fitting a polynomial to three consecutive gantry angles and differentiating twice:

$$|2(\theta_{k+1} - \theta_k)\Delta t_{k-1} - 2(\theta_k - \theta_{k-1})\Delta t_k| \leq \ddot{\theta}_{max}\left(\Delta t_{k-1}^2 \Delta t_k + \Delta t_k^2 \Delta t_{k-1}\right),$$

for all k. Successive Linear Programming (SLP) is used to handle the acceleration constraint.

4.5. Constraints to sort projections in increasing gantry angle order

To model the objectives we need the M_b gantry angles in each respiratory bin in increasing order. We choose to use an assignment, or bipartite matching, formulation to order the gantry angles. In each respiratory bin, b, we let $\theta_{b,l}$ be the ordered gantry angles with $\theta_{b,l+1} \geq \theta_{b,l}$ for all b and $l = 1, 2, \ldots, M_b$. We introduce binary variables $x_{b,k,l}$ that take the value 1 if θ_k is the l^{th} largest gantry angle in respiratory bin b and zero otherwise:

$$\begin{aligned}
\sum_{k=1}^{M} \theta_k x_{b,k,l} &= \theta_{b,l} \text{ for all } b \text{ and } l, \\
\sum_{k=1}^{M} x_{b,k,l} &= 1 \text{ for all } b \text{ and } l, \\
\sum_{l=1}^{M_b} x_{b,k,l} &= 1 \text{ for all } b \text{ and } k. \\
x_{b,k,l} &\leq \delta_{b,k} \text{ for all } b, l \text{ and } k.
\end{aligned} \tag{4}$$

‡ Personal communication with Scott Johnson, Sr Manager, Research Collaborations, Varian Medical Systems, 5 September 2012.

In equation (4) we have the product of a continuous and binary variable. We use the following well know technique to linearise the product. Let x be a binary variable and $0 \leq y \leq y_{max}$ be a continuous variable, then the product $z = xy$ can be linearised with

$$z \geq 0,\ z \leq y_{max},\ z \leq y \text{ and } z \geq y - (1-x)y_{max}.$$

4.6. Objectives

There are two objectives that we use:

(i) Given that we take M_b projections per respiratory bin, minimise the root mean square (RMS) of the angular separation between projections. This will also require an additional constraint on the total imaging time, t_{max}, to make sure that the total imaging time is acceptable.

(ii) Minimise the total imaging time, t_{max}, where the imaging time is the total time required to acquire a set of projections with a specified angular separation between the projections.

4.6.1. Minimising the RMS of the angular separation between projections: The ideal angular separation between projections is $\Delta\theta_b = 2\pi/M_b$. The RMS of the angular separation between projections in bin b is given by

$$RMS_b^2 = \left[\sum_{l=1}^{M_b-1} (\theta_{b,l+1} - \theta_{b,l} - \Delta\theta_b)^2 + (2\pi - (\theta_{b,M_b} - \theta_{b,0}) - \Delta\theta_b)^2\right]/M_b, \quad (5)$$

for all b. The objective can be written as

$$\text{RMS}^2 = \text{Minimise } \sum_{b=1}^{N} RMS_b^2. \quad (6)$$

This is a quadratic objective and can be solved with the quadratic solvers in most commercial MIQP optimization packages. As an alternative, we could minimise the RMS from the ideal gantry angles

$$RMS_b^2 = \left[\sum_{l=1}^{M_b} (\theta_{b,l} - l\Delta\theta_b)^2\right]/M_b \text{ for all } b.$$

For full fan acquisition, the angular separation is $\Delta\theta_b = (\pi + \omega)/M_b$, so that equation (5) becomes

$$RMS_b^2 = \left[\sum_{l=1}^{M_b-1} (\theta_{b,l+1} - \theta_{b,l} - \Delta\theta_b)^2 + (\pi + \omega - (\theta_{b,M_b} - \theta_{b,0}) - \Delta\theta_b)^2\right]/M_b,$$

for all b.

4.6.2. Minimising the total imaging time, t_{max}: In this case, the objective is

$$\text{minimise } t_M = \text{minimise } t_{max}. \tag{7}$$

However, we need to specify additional constraints to guarantee that we collect sufficient projections for image reconstruction. If we take M_b projections per respiratory bin, with an angular separation of exactly $\Delta\theta_b = 2\pi/M_b$ (for full fan acquisition $\Delta\theta_b = (\pi + \omega)/M_b$), then

$$M_b = \sum_{k=1}^{M} \sum_{j=1}^{N_b} \delta_{b,j,k} \text{ for all } b, \tag{8}$$

$$\Delta\theta_b = \theta_{b,l+1} - \theta_{b,l} \text{ for } l = 1, 2, \ldots, M_b - 1, \tag{9}$$

$$\Delta\theta_b = 2\pi - (\theta_{b,M_b} - \theta_{b,0}) \text{ for half fan acquisition.} \tag{10}$$

$$\Delta\theta_b = \pi + \omega - (\theta_{b,M_b} - \theta_{b,0}) \text{ for full fan acquisition.}$$

Alternatively we could introduce a range for the gantry angles by replacing equations (9) and (10) with

$$l\Delta\theta_b - \epsilon \leq \theta_{b,l} \leq l\Delta\theta_b + \epsilon \text{ for all } l,$$

where ϵ is an allowable tolerance on the ideal gantry angle.

5. Solution Methods

The MIQP model has been implemented using the three leading commercial MIQP solvers (ILOG CPLEX, XPRESS-MP and GUROBI). The linear relaxation of the problem is poor and all three commercial solvers fail to obtain optimal solutions to problems with any more than a small number of projections per respiratory bin. Although obtaining a provably optimum solution is difficult, we can make considerable progress using heuristic methods that generate a near optimal solution in a short period of time.

We will call our heuristic solution method the single gantry rotation (SGR) heuristic because the gantry is restricted to a single rotation. Details on the implementation of the SGR heuristic together with details on how to simulate conventional 4DCBCT are given in Appendix A. To assess the accuracy of the SGR heuristic a more complex heuristic, the 2-opt exchange heuristic, that has a computation time of approximately one day, has been implemented. The details of the 2-opt exchange heuristic are given in Appendix A. We will analyse the performance of the SGR heuristic, conventional 4DCBCT and the 2-opt exchange heuristic.

6. Results and Analysis

We expect the RMS, as defined by equation 6, to be smaller for larger values of M_b. For example, if we acquire $M_b = 240$ projections per respiratory bin the projections will be closer together, and the RMS will likely be smaller, than if we acquire 60 projections per respiratory bin. This makes it difficult to compare solution quality for different values

of M_b. An alternative measure of the RMS can be obtained by scaling equation 6 to give the scaled RMS

$$\text{Scaled RMS} = 100 \left[\sum_{b=1}^{N} RMS_b^2 / (\Delta\theta_b^2 N) \right]^{1/2}.$$

A scaled RMS of zero means that there is perfect angular spacing between projections. A scaled RMS of 100 means that the RMS between projections is $\Delta\theta_b$; we are likely to see two, or more, projections with a similar gantry angle followed by a gap of approximately $2\Delta\theta_b$.

In our numerical experiments the default, or baseline, settings are $M_b = 120$ half fan projections per respiratory bin, $N = 10$ respiratory bins (1200 projections in total), the projections are taken over $t_{max} = 240$ seconds, the maximum gantry acceleration is $1.8°/s^2$ and the maximum gantry velocity is $6°/s$. The default settings represent the settings used clinically on the Elekta 4DCBCT system with the acceleration limit the smallest acceleration measured by (Boylan et al. 2011) and the I.E.C. velocity limit.

6.1. RMG-4DCBCT Compared with Conventional 4DCBCT

To examine the performance of RMG-4DCBCT compared to conventional 4DCBCT for both current and future generation systems, we have run simulations with maximum velocities of 6, 10, 15 and $30°/s$, and maximum accelerations of 1.8, 3, 6 and $12°/s^2$. We have also run simulations where the total number of projections have been reduced to as low as 60 projections per respiratory bin. Table 1 compares the results between RMG-4DCBCT using the SGR heuristic and conventional 4DCBCT. We report on the results for displacement and phase binning in the next two sections.

6.1.1. Displacement binning: Increasing the maximum gantry acceleration from $1.8°/s^2$ to $12°/s^2$ improves the scaled RMS from 21.2 to 0.3 with RMG-4DCBCT (rows 1 to 4) while conventional 4DCBCT has a scaled RMS of 90.9. It should be noted that conventional 4DCBCT has a different number of projections in each respiratory bin while RMG-4DCBCT has exactly 120 projections per bin. Increasing the maximum velocity of the gantry to $30°/s$ does not improve the scaled RMS (rows 5 to 7). An explanation is that the gantry makes only one rotation with an average angular velocity of $1.5°/s$. Even if the gantry accelerates and decelerates it rarely goes above $6°/s$. These results clearly show that increasing the maximum acceleration of the gantry is more important than increasing the maximum velocity of the gantry.

Rows 8 to 10 correspond to 4, 6 and 8 respiratory bins. The results show that conventional 4DCBCT gives a scaled RMS around 63 or 64 for all simulations while the (unscaled) RMS increases with the number of respiratory bins. RMG-4DCBCT has a lower scaled RMS when the number of respiratory bins are reduced. When the patient has a longer breathing period, rows 11 to 13, the scaled RMS for conventional 4DCBCT increases. The scaled RMS with the RMG-4DCBCT is much lower than the scaled RMS for conventional 4DCBCT for all breathing periods used.

Table 1. The scaled RMS and unscaled RMS in brackets for RMG-4DCBCT (using the RMG heuristic) compared to conventional 4DCBCT. The patients breathing period is ω seconds and the conventional 4DCBCT column with a * indicates that not all respiratory bins had the same number of projections; for the patient with a breathing period of two seconds two displacement bins had zero projections. NA indicates that the simulation was not applicable for the parameter settings.

					Proj		Displacement Binning		Phase Binning	
Row	ω		Vel	Acc	per	t_{max}	Conven-	RMG-	Conven-	RMG-
	sec	Bins	°/s	°/s^2	bin	sec	tional*	4DCBCT	tional	4DCBCT
1	4.0	10	6	1.8	120	240	90.9(2.7°)	21.2(0.6°)	90.0(2.7°)	84.1(2.5°)
2	4.0	10	6	**3.0**	120	240	90.9(2.7°)	12.3(0.4°)	90.0(2.7°)	83.5(2.5°)
3	4.0	10	6	**6.0**	120	240	90.9(2.7°)	2.0(0.1°)	90.0(2.7°)	82.0(2.5°)
4	4.0	10	6	**12.0**	120	240	90.9(2.7°)	0.3(0.0°)	90.0(2.7°)	78.5(2.4°)
5	4.0	10	**10**	1.8	120	240	90.9(2.7°)	21.2(0.6°)	90.0(2.7°)	84.1(2.5°)
6	4.0	10	**15**	1.8	120	240	90.9(2.7°)	21.2(0.6°)	90.0(2.7°)	84.1(2.5°)
7	4.0	10	**30**	1.8	120	240	90.9(2.7°)	21.2(0.6°)	90.0(2.7°)	84.1(2.5°)
8	4.0	**4**	6	1.8	120	240	62.8(1.3°)	7.6(0.2°)	75.2(2.3°)	52.4(1.6°)
9	4.0	**6**	6	1.8	120	240	64.2(1.4°)	14.9(0.4°)	83.3(2.5°)	70.0(2.1°)
10	4.0	**8**	6	1.8	120	240	64.1(2.7°)	18.5(0.6°)	87.6(2.6°)	78.8(2.4°)
11	**6.0**	10	6	1.8	120	240	91.0(2.0°)	6.8(0.2°)	127.4(3.8°)	123.1(3.7°)
12	**3.3**	10	6	1.8	120	240	71.7(2.2°)	21.7(0.7°)	73.6(2.2°)	70.8(2.1°)
13	**2.0**	10	6	1.8	120	240	35.9(0.5°)	0.0(0.0°)	0.0(0.0°)	0.0(0.0°)
14	4.0	10	6	1.8	**60**	**120**	90.9(5.5°)	28.2(1.7°)	90.0(5.4°)	84.6(5.1°)
15	4.0	10	6	1.8	**200**	**400**	90.9(1.6°)	12.7(0.2°)	90.0(1.6°)	83.5(1.5°)
16	4.0	10	6	1.8	120	**160**	NA	NA	127.3(3.8°)	113.5(3.8°)
17	4.0	10	6	1.8	120	**180**	NA	NA	116.2(3.5°)	102.9(3.5°)
18	4.0	10	6	1.8	120	**200**	NA	NA	108.9(3.3°)	84.8(3.3°)

Decreasing the number of projections to 60 with an imaging time of 120 seconds, row 14, or, increasing the number of projections to 200 with an imaging time of 400 seconds, row 15, has the same average time between projections, 0.2 seconds, as the default case. Using RMG-4DCBCT we find the scaled RMS is smaller for $M_b = 200$ than for $M_b = 60$. This is because the projections are closer together and less extreme changes in velocity and acceleration are required to spread out the projections.

6.1.2. Phase binning: When phase based binning is used the results follow a similar pattern, but the improvement of RMG-4DCBCT over conventional 4DCBCT is not as significant as the displacement binning results. For the default case, with displacement binning, there is a reduction in the RMS of 77.4% while the reduction in the RMS for phase binning is 6.6%. An explanation is that for the default case, with displacement binning, only one projection per time window occurs for all time windows except the time windows at inhale and exhale limit. In comparison, two projections are taken, in a short time period, in each time window when phase based binning is used. Only one gantry rotation is allowed so the velocity of the gantry is low, on average $1.5°/s$,

Table 2. Comparison of RMG-4DCBCT heuristic methods. The scaled RMS (and unscaled RMS in brackets) with the SGR heuristic and the 2-opt exchange heuristic. In all simulations it was assumed that the patient had a four second breathing period and there were 10 respiratory bins. M_b is the number of projections per respiratory bin and t_{max} is the total imaging time.

	t_{max}	Vel	Acc	Displacement Binning		Phase Binning	
M_b	sec	°/s	°/s^2	SGR	2-opt	SGR	2-opt
120	240	6	1.8	21.2(0.6°)	21.2(0.6°)	84.1(2.5°)	84.1(2.5°)
120	240	30	3.0	12.3(0.4°)	12.3(0.4°)	83.5(2.5°)	81.6(2.5°)
120	240	30	6.0	2.0(0.1°)	2.0(0.1°)	82.0(2.2°)	73.2(2.2°)
100	200	6	1.8	23.8(0.7°)	23.8(0.7°)	84.3(2.5°)	84.3(2.5°)
100	200	30	3.0	16.4(0.5°)	16.4(0.5°)	83.8(2.5°)	83.6(2.5°)
100	200	30	6.0	5.5(0.2°)	5.5(0.2°)	82.5(2.5°)	78.9(2.4°)
50	100	6	1.8	29.9(0.9°)	29.9(0.9°)	84.6(2.5°)	84.6(2.5°)
50	100	30	3.0	26.0(0.8°)	26.0(0.8°)	84.4(2.5°)	84.4(2.5°)
50	100	30	6.0	16.9(0.5°)	16.9(0.5°)	83.8(2.5°)	83.8(2.5°)
50	200	6	1.8	2.4(0.1°)	0.2(0.0°)	0.1(0.0°)	0.0(0.0°)
50	200	30	3.0	1.5(0.1°)	1.2(0.0°)	0.1(0.0°)	0.0(0.0°)
50	200	30	6.0	0.1(0.0°)	0.0(0.0°)	0.0(0.0°)	0.0(0.0°)

and the angular separation between the two projections in each time window is small. The implication for phase based binning is that it is difficult to reduce the scaled RMS without increasing the imaging time. The main advantage of RMG-4DCBCT over conventional 4DCBCT is that RMG-4DCBCT guarantees 120 projections in every respiratory bin while conventional 4DCBCT does not guarantee 120 projections per respiratory bin.

When a patient has a two second breathing period, and phase based binning is used, conventional 4DCBCT is optimal. In this case, one projection per time window occurs and a constant angular velocity of $1.5°/s$ positions the gantry in an ideal position to take the next projection.

One benefit of phase based binning, over displacement binning, is that due to the longer time windows for each respiratory bin we can reduce the imaging time. We examine shorter time periods in the last three rows in table 1. The results show that reducing the imaging time to 200 seconds does not significantly increase the scaled RMS over the default, 240 second, imaging time. However, reducing the imaging time to 180 seconds, or less, results in a moderate increase in the scaled RMS.

6.2. The 2-opt Exchange Heuristic versus the SGR Heuristic

Table 2 gives the RMS and scaled RMS for the SGR heuristic and 2-opt exchange heuristic for a variety of different parameter settings. In rows 1 to 9, with displacement binning, the 2-opt exchange heuristic did not improve the solution where, on average, one projection is taken per time window. However when there are only 50 projections in

200 seconds, on average one projection every second time window, the 2-opt exchange heuristic is able to improve the solution from the SGR heuristic. The explanation is that there are many time windows that do not have projections allocated and the 2-opt exchange heuristic is able to better determine the time windows that should not have projections allocated.

It should be noted that the improvements to the solution are only small or moderate when using the 2-opt exchange heuristic to improve the SGR heuristic. We therefore expect the SGR heuristic to produce a good solution in most cases, with an acceptable computation time, but further improvements are possible especially if the maximum acceleration of the gantry is high.

6.3. Image Quality for Different Values of the Scaled RMS

To examine the image quality for different values of the scaled RMS the Catphan phantom has been used to reconstruct CBCT images. The full data set of the Catphan phantom consists of 608 half fan projections which we sample to produce the images in this section. The results corresponding to row 1 in Table 1 are given in Figure 4. For conventional 4DCBCT with displacement binning there is no guarantee of obtaining 120 projections in each respiratory bin, so we have selected the respiratory bins with the least and most projections; both of these respiratory bins have a scaled RMS above the RMS of 90.9 which is obtained across all 10 respiratory bins.

The image quality degrades for increased values of the scaled RMS with the streak artefacts increasing with larger values of the scaled RMS. With displacement binning, RMG-4DCBCT achieves better image quality than conventional. For conventional 4DCBCT with displacement binning, the respiratory bin with the least number of projections (78 projections) has severe streak artefacts. This is primarily due to insufficient data from the large gaps between the clusters of projections. For phase binning, similar image quality is obtained with both RMG-4DCBCT and conventional 4DCBCT. However, these results represent a best case scenario for conventional 4DCBCT as the respiratory signal is sinusoidal and not irregular.

7. Discussion

Our results show that RMG-4DCBCT is a promising method for reducing the clustering of projections that occurs in conventional 4DCBCT. We have shown that the RMS between projections is reduced by 77.4% when using displacement binning with a 6.6% reduction in RMS when phase based binning is used. We have demonstrated that a high gantry acceleration is more important than a high gantry velocity, which is an important consideration when designing hardware to implement RMG-4DCBCT.

Our analysis of images for different values of the gantry angle RMS in Figure 4 demonstrates that when projections are more uniformly spaced fewer projections are required to produce images of suitable quality for use in radiotherapy. We also observed

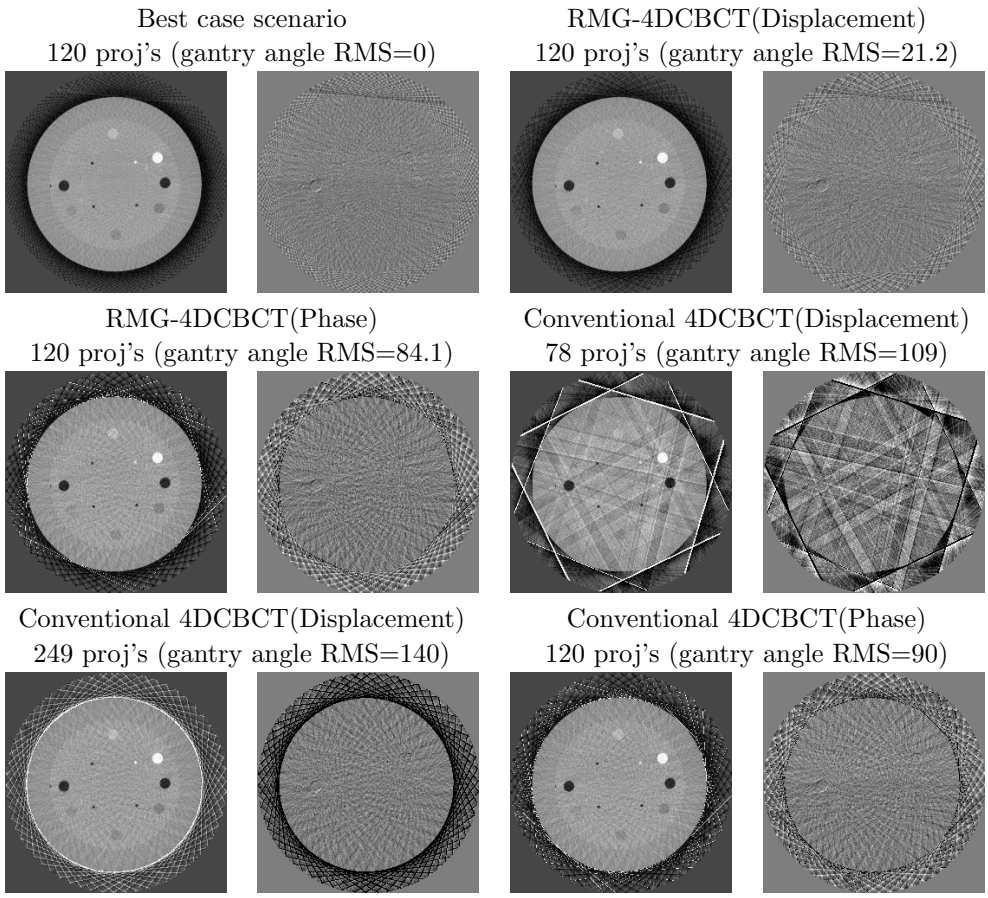

Figure 4. CBCT images of the Catphan phantom from the data in row 1 of Table 1. For each pair of images, the image on the right is the difference image generated by subtracting the image on the left from an image generated with the full 608 projection dataset. The number of projections in each respiratory bin with conventional 4DCBCT using displacement binning varies depending on the breathing rate; the bins with the least and most projections have been used for conventional 4DCBCT with displacement binning.

in Figure 4 that conventional 4DCBCT does not guarantee enough projections in each respiratory bin to reconstruct an image. Our primary motivation for this study was to obtain clinically useful images by delivering a lower radiation dose to the patient. However, additional benefits of RMG-4DCBCT over conventional 4DCBCT is that the images are of a higher quality when the same number of projections are used and every respiratory bin will have the same number of projections.

Our results suggest that displacement binning is likely to produce better angular separation between projections for 4DCBCT imaging, and could potentially produce better quality images for the same number of projections, than phase based binning. In addition, it has been concluded that displacement binning is more accurate than phase binning in a phantom study comparing phase and displacement binning for 4DCT (Abdelnour et al. 2007). Although phase binning is common practice for 4DCT, these results suggest that displacement binning is worth pursuing for both 4DCT and

4DCBCT imaging. However, several practical considerations need to be addressed before changing clinical practice and switching to displacement binning. These include the shorter time period spent in the respiratory bins in the middle of the breathing cycle, baseline drifts of the respiratory signal, the corresponding difficulties attempting to take a projection in a smaller time window and problems associated with collecting missed projections in the inhale or exhale limit respiratory bins if a patient takes a shallow breath.

An additional complication is that it is unclear if errors could occur if phase binning is used during treatment planning for 4DCT while displacement binning is used to position the patient for treatment with 4DCBCT. If 4DCT images are obtained by retrospectively sorting projections into respiratory bins, then the image quality using both phase and displacement binning can be assessed on a patient by patient basis with the best binning method being used during treatment to acquire 4DCBCT images.

From an optimization point of view further progress towards generating a global optimal solution to the full MIQP model would be useful. For large MIQP models, a global solution is often impossible to obtain so heuristic methods are used to generate a near optimal solution with a short computation time. There are two avenues for future work: (1) Generating a better solution to the full MIQP model without consideration of computation time. Possible approaches include reformulating the model, cut generators for the branch and bound algorithm and meta heuristics such as evolutionary algorithms. Even if a solution takes days or months to compute, it gives useful insight into how the SGR heuristic can be improved. (2) Develop novel heuristics that generate better solutions to the MIQP than the SGR heuristic with a solution time of under 4 seconds. Possible approaches include exchange heuristics or a tailored search algorithm. These heuristics could replace the SGR heuristic in the implementation of RMG-4DCBCT.

Throughout this study we have made comparisons between conventional 4DCBCT and RMG-4DCBCT when the same number of projections are acquired per respiratory bin. That is, if conventional 4DCBCT acquires an average of 120 projections per respiratory bin then we made a direct comparison with RMG-4DCBCT acquiring 120 projections per respiratory bin. In practice, with better angular separation between projections using RMG-4DCBCT, fewer projections are required per respiratory bin than for conventional 4DCBCT. For example, the phase based binning results had a scaled RMS of around 85 because two projections were acquired per respiratory cycle. However, we could acquire one projection per respiratory cycle, for a total of 50 respiratory cycles, to obtain a much smaller scaled RMS. In addition, to further reduce imaging dose to the patient, RMG-4DCBCT could be used with modern iterative reconstruction techniques that show promise in reducing the number of projections required to reconstruct images (Bian et al. 2010).

One limitation of this study is that we have focused on sinusoidal breathing traces rather than real patient breathing traces. In practice a representative breathing trajectory will be used to optimize the gantry velocity and projection time interval schedule with the maximum velocity and acceleration constraints being applied to

the representative breathing trajectory. A sinusoidal breathing wave is a potential candidate for the representative breathing trajectory with the computed gantry velocity and projection time interval schedule being a function of the respiratory signal (e.g. phase or displacement) and not time. When image acquisition starts the patient's actual respiratory signal is compared to the representative breathing trajectory with the gantry's velocity adjusted according to the real time respiratory signal. If the patient starts breathing faster than the speed of the representative breathing trajectory then the gantry is moved faster. If the patient starts breathing slower than the speed of the representative breathing trajectory then the gantry is moved slower. On average, for the default parameters, the gantry moves at $1.5^\circ/s$ so the patient would need to breathe four times faster (i.e. a one second breathing period compared to a 4 second breathing period) than the representative breathing trajectory to move the gantry at a speed close to $6^\circ/s$. A buffer on the maximum velocity and acceleration, or a faster representative breathing trajectory, can be used to reduce, or eliminate, maximum velocity and acceleration violations that could occur if the patient starts breathing very fast.

If the patient's breathing becomes irregular, we stop acquisition, wait for the patient's breathing to settle down, recompute a new schedule and continue acquisition. It is therefore important to be able to quickly recompute a projection schedule as any delays increase the imaging time, and discomfort, to the patient. Ideally, this would take less than one second, but the length of a breathing cycle, typically 4 seconds, is acceptable. The SGR heuristic presented above has the advantage that a solution can be obtained in under one second.

There have been some attempts to determine if breathing is irregular or if it is chaotic (Tewatia et al. 2011). In either case, if breathing is irregular or chaotic, it is very difficult to predict a patient's breathing for one or two cycles ahead. Predicting a patient's breathing for the entire duration of a CBCT scan is even more difficult. To overcome the problems associated with irregular breathing some studies have used audio and visual queues to guide the patient's breathing (Kini et al. 2003, George et al. 2006, Venkat et al. 2008). These systems typically monitor external markers on a patient's abdomen to provide near real-time data on the patient's breathing. A representative breathing wave is computed during a training phase and then the patient attempts to follow the representative breathing wave with both audio and visual queues. In a study where 90 respiratory traces were acquired from 10 patients the root mean squared variation in displacement is reduced from 0.16cm with free breathing to 0.08cm with audiovisual biofeedback and the root mean squared variation in the breathing period is reduced from 0.77s with free breathing to 0.2s with audiovisual biofeedback (Venkat et al. 2008). However, there has not been a study to determine if audiovisual biofeedback improves 4DCBCT imaging.

In the final implementation of RMG-4DCBCT system latencies need to be considered. There are three dominate sources of latency: (1) The signal from the respiratory system. One common respiratory monitoring system is the Varian RPM system with a frequency of 33ms. (2) The time required to compare the real-time

respiratory signal with the representative breathing trajectory is less than 10ms on modern computers. (3) The time required to send a command to the gantry and for the gantry to respond is currently unknown. The overall latency is unknown but, as a guide, we can look at applications that incorporate an RPM sensor and move the leaves on the multi leaf collimator where the delay has been measured at between 88.3 and 90.5ms (Duan et al. 2003). Errors arising due to these latencies can be mitigated by predicting the respiratory signal so that the gantry can be moved accordingly. In a study comparing four different prediction methods with a variety of different input frequencies, over prediction intervals ranging in size from 0.2 to 0.6 seconds, it has been shown that the prediction methods roughly halve the position errors compared to using no prediction (Krauss et al. 2011).

8. Conclusions

We have described RMG-4DCBCT for the first time. RMG-4DCBCT uses the respiratory signal to regulate the gantry velocity and projection time interval to improve 4DCBCT imaging. The method is a promising approach to reduce, or eliminate, projection clustering that exists in current generation 4DCBCT systems. Because less projections are required there is potential to reduce the overall imaging time and the imaging dose to the patient.

This paper has focused on one aspect of RMG-4DCBCT which is to optimize the gantry velocity and projection time interval schedule; a key step on the path to implement RMG-4DCBCT. A simple heuristic method has been presented that can generate a near optimal projection schedule in under one second. It was shown that RMG-4DCBCT reduces the angular separation between projections over conventional 4DCBCT.

Acknowledgments

Professor Keall would like to acknowledge the support of a National Health and Medical Research Council (NHMRC) Australia Fellowship. This project was supported in part by NHMRC project grant 1034060. The authors would like to thank Fair Isaacs Corporation (FICO), IBM-ILOG and GUROBI optimization for academic licenses to XPRESS-MP, CPLEX and GUROBI respectively. This material is the subject of US patent application PCT/US2012/048693 and provisional patent application 61/671028.

Appendix A. Solution Methods

Appendix A.1. The Single Gantry Rotation (SGR) Heuristic

The heuristic presented in this section is used to generate an initial feasible solution to the MIQP model. The heuristic can be implemented in under one second using

the Newton Barrier method in most Quadratic Programming (QP) packages such as CPLEX, XPRESS and GUROBI.

There are two simplifications to the model that eliminate the binary variables and allow the problem to be solved efficiently. First, if we assume that a given number of projections, $\mathcal{K}(b,j)$, will be taken in each time window, $R_{b,j}$, then we do not need the binary variables, $\delta_{b,j,k}$, that determine which respiratory bin the projections belong. We can use $\mathcal{K}(b,j)$ in a pre-processing phase to determine the time window that the projection taken at time t_k belongs and then we apply the constraint

$$ts(b,j) \leq t_k \leq te(b,j) \text{ for projection } k \text{ in respiratory bin } R(b,j).$$

The easiest way to allocate projections to time windows is to evenly distribute the projections across the time windows, $R(b,j)$. That is, we take $\lfloor M_b/N_b \rfloor$ projections per time window with the remaining $M_b - \lfloor M_b/N_b \rfloor$ evenly spaced across the time windows§. The maximum number of projections per time window can be calculated using $\mathcal{K}(b,j) \leq 1 + (te_{b,j} - ts_{b,j})/\Delta t_{min}$.

The second simplification eliminates the binary variables, $x_{b,k,l}$, which were used in section 4.5 to order the projections within each respiratory bin. Within each respiratory bin, we force the gantry to take projections with an increasing gantry angle (i.e. only one gantry rotation). That is, we apply the constraint $\theta_{b,j+1} \geq \theta_{b,j}$ for all values of j. This does not restrict the gantry from changing direction between respiratory bins; the condition ensures that consecutive projections within the same respiratory bin are taken in increasing gantry angle order. We use the notation $\mathcal{M} : k \rightarrow (b,l)$ which maps a projection, θ_k taken at time t_k, to its corresponding ordered projection $\theta_{b,l}$. That is, $\mathcal{M}$ takes a value of k and maps it to a unique pair (b,l) so that $\theta_k = \theta_{b,l}$. Every k must map to a unique pair (b,l) and every (b,l) has a corresponding value of k. We can create the mapping $\mathcal{M}$ in a pre-processing phase before performing the optimization.

Pseudo code of the methods used to initialise $\mathcal{M}$ and $\mathcal{K}$ are given in algorithm 1. Pseudo code to compute the objective given the mappings for $\mathcal{M}$ and $\mathcal{K}$ is given in algorithm 2.

Appendix A.2. Conventional 4DCBCT

Current generation 4DCBCT techniques are based on a constant angular gantry velocity with a constant projection pulse rate. The velocity of the gantry is calculated by dividing 360° by the total amount of time that is allocated at the start of 4DCBCT imaging to acquire all of the projections (the imaging time). For example, if an imaging time of 240 seconds is used then the velocity of the gantry is $1.5°/s$. Similarly, the projection pulse rate can be determined by dividing the imaging time by the total number of projections (projections per bin multiplied by the number of respiratory bins). For example, if 10 respiratory bins are used with an average of 120 projections per bin then the projection pulse rate is 0.2 seconds.

§ $\lfloor x \rfloor$ means that we use the largest integer less than x.

Algorithm 1 SGR Heuristic.

{Initialise $\mathcal{K}$.}
for $b = 1$ **to** N **do**
  $n = \lfloor M_b/N_b \rfloor$; $\delta n = M_b - nN_b$; $\delta j = M_b/\delta n$
  for $j = 1$ **to** M_b **do**
    $\mathcal{K}(b, j) = n$
  end for
  for $i = 1$ **to** δn **do**
    $j = \lfloor (i-1)\delta j \rfloor$; $\mathcal{K}(b, j) = \mathcal{K}(b, j) + 1$
  end for
end for
{Initialise $\mathcal{M}$.}
$k = 0$
for $b = 1$ **to** M_b **do**
  $L[b] = 0$
end for
Order projection counts, $\mathcal{K}(b, j)$, from lowest to highest $ts_{b,j}$ to get $\mathcal{K}'(b, j)$.
for all (b, j) in $\mathcal{K}'$ **do**
  for $i = 1$ **to** $\mathcal{K}'(b, j)$ **do**
    $l = L[b]$; $\mathcal{M}(k) = (b, l)$; $L[b] = L[b] + 1$; $k = k + 1$
  end for
end for
Optimize($\mathcal{M}, \mathcal{K}$)

Algorithm 2 Optimize($\mathcal{M}, \mathcal{K}$).

{Check if values exist.}
if Cache.Contains($\mathcal{M}, \mathcal{K}$) **then**
  objective = Cache($\mathcal{M}, \mathcal{K}$)
else
  {Formulate QP by excluding sections 4.3 and 4.5.}
  for $k = 1$ **to** M **do**
    $(b, l) = \mathcal{M}(k)$
    Add constraint $\theta_{b,l} = \theta_k$
  end for
  k = 1
  for $b = 1$ **to** N **do**
    for $j = 1$ **to** M_b **do**
      for $i = 0$ **to** $\mathcal{K}(b, j)$ **do**
        Add constraint $ts_{b,j} \leq t_k \leq te_{b,j}$
        $k = k + 1$
      end for
    end for
  end for
  objective = Solve() - using XPRESS-MP, CPLEX or GUROBI
  Cache($\mathcal{M}, \mathcal{K}$) = *objective*
end if
return *objective*

Appendix A.3. The 2*-opt Exchange Heuristics*

The k-opt exchange heuristic is a simple heuristic that performs a local search around a known solution. More information on the implementation and design of meta heuristics can be found in (Talbi 2009). For our application we keep the computation time down by using $k = 2$. The 2-opt exchange heuristic systematically swaps two projections from one time window to another by altering the mapping $\mathcal{K}$, or, adjusting the order of the mapping $\mathcal{M}$. The new mappings for $\mathcal{M}$ and $\mathcal{K}$ are optimized and accepted as an improved solution if the mapping improves the objective.

The 2-opt exchange heuristic is easy to implement but the solution time is too slow to use in practice. The purpose is to perform a local search around the solution obtained from the SGR heuristic and to determine if effort should be spent developing more complicated heuristics. For each simulation it takes about one day of computation time to prove that the solution is 2-optimal; meaning it is not possible to swap two

projections and improve the solution.

References

Abdelnour A F, Nehmeh S A, Pan T, Humm J L, Vernon P, Schoder H, Rosenzweig K E, Mageras G S, Yorke E, Larson S M & Erdi Y E 2007 Phase and amplitude binning for 4D-CT imaging *Phys Med Biol* **52**(12), 3515–29.

Bian J, Siewerdsen J H, Han X, Sidky E Y, Prince J L, Pelizzari C A & Pan X 2010 Evaluation of sparse-view reconstruction from flat-panel-detector cone-beam CT *Phys Med Biol* **55**(22), 6575–99.

Boylan C J, Rowbottom C G & Mackay R I 2011 The use of a realistic VMAT delivery emulator to optimize dynamic machine parameters for improved treatment efficiency *Physics in Medicine and Biology* **56**(13), 4119–4133.

Boyle P & Levin B 2008 World Cancer Report 2008 *World Health Organization* .

Delaney G, Jacob S, Featherstone C & Barton M 2005 The role of radiotherapy in cancer treatment: estimating optimal utilization from a review of evidence-based clinical guidelines *Cancer* **104**(6), 1129–37.

Duan J, Shen S, Fiveash J, Brezovich I, Popple R & Pareek P 2003 Dosimetric effect of respiratory-gated beam on IMRT delivery *Med Phys* **30**(8), 2241–52.

Feldkamp L A, Davis L C & Kress J W 1984 Practical Cone-Beam Algorithm *Journal of the Optical Society of America a-Optics Image Science and Vision* **1**(6), 612–619.

George R, Chung T D, Vedam S S, Ramakrishnan V, Mohan R, Weiss E & Keall P J 2006 Audio-visual biofeedback for respiratory-gated radiotherapy: impact of audio instruction and audio-visual biofeedback on respiratory-gated radiotherapy *Int J Radiat Oncol Biol Phys* **65**(3), 924–33.

Kini V R, Vedam S S, Keall P J, Patil S, Chen C & Mohan R 2003 Patient training in respiratory-gated radiotherapy *Med Dosim* **28**(1), 7–11.

Krauss A, Nill S & Oelfke U 2011 The comparative performance of four respiratory motion predictors for real-time tumour tracking *Phys Med Biol* **56**(16), 5303–17.

Leng S, Zambelli J, Tolakanahalli R, Nett B, Munro P, Star-Lack J, Paliwal B & Chen G H 2008 Streaking artifacts reduction in four-dimensional cone-beam computed tomography *Med Phys* **35**(10), 4649–59.

Machtay M, Bae K, Movsas B, Paulus R, Gore E M, Komaki R, Albain K, Sause W T & Curran W J 2012 Higher biologically effective dose of radiotherapy is associated with improved outcomes for locally advanced non-small cell lung carcinoma treated with chemoradiation: an analysis of the Radiation Therapy Oncology Group *Int J Radiat Oncol Biol Phys* **82**(1), 425–34.

Marks L B, Bentzen S M, Deasy J O, Kong F M, Bradley J D, Vogelius I S, El Naqa I, Hubbs J L, Lebesque J V, Timmerman R D, Martel M K & Jackson A 2010 Radiation dose-volume effects in the lung *Int J Radiat Oncol Biol Phys* **76**(3 Suppl), S70–6.

Simpson D R, Lawson J D, Nath S K, Rose B S, Mundt A J & Mell L K 2010 A Survey of Image-Guided Radiation Therapy Use in the United States *Cancer* **116**(16), 3953–3960.

Sonke J J, Zijp L, Remeijer P & van Herk M 2005 Respiratory correlated cone beam CT *Medical Physics* **32**(4), 1176–1186.

Taguchi K 2003 Temporal resolution and the evaluation of candidate algorithms for four-dimensional CT *Medical Physics* **30**(4), 640–650.

Talbi E G 2009 *Metaheuristics: From Design to Implementation (Wiley Series on Parallel and Distributed Computing)* John Wiley and Sons. Hoboken, New Jersey.

Tewatia D K, Tolakanahalli R P, Paliwal B R & Tome W A 2011 Time series analyses of breathing patterns of lung cancer patients using nonlinear dynamical system theory *Physics in Medicine and Biology* **56**(7), 2161–2181.

Venkat R B, Sawant A, Suh Y L, George R & Keall P J 2008 Development and preliminary evaluation

of a prototype audiovisual biofeedback device incorporating a patient-specific guiding waveform *Physics in Medicine and Biology* **53**(11), N197–N208.